SPACE ENVIRONMENTAL EFFECTS ON POLYMER MATRIX COMPOSITES AS A FUNCTION OF SAMPLE LOCATION ON LDEF

R. C. Tennyson and G. R. Cool
University of Toronto Institute for Aerospace Studies
North York, Ontario, Canada, M3H 5T6

D. G. Zimcik
Canadian Space Agency, Space Mechanics Directorate
Ottawa, Ontario, Canada, K2H 8S2

SUMMARY

This paper presents results on the effect of circumferential location on the variation in solar absorptance (α_s) and infrared emittance (ε) for five different polymer matrix composites (PMC), and variations in erosion depth due to atomic oxygen (AO) for fourteen different PMC materials. In addition, a chemical content design parameter (γ) has been found that correlates well with the erosion yield obtained from space flight data and hyperthermal AO tests for hydrocarbon polymeric materials. This parameter defines the ratio of the total number of atoms in a repeat monomer unit to the difference between the total carbon content and the total number of intermolecular oxygen atoms in the same repeat unit.

INTRODUCTION

The purpose of this report is to present a survey of the polymer matrix composite materials that were flown on LDEF with particular attention to the effect of circumferential location (θ) on the measured degradation and selected property changes (see Fig. 1). Specifically, it is known that atomic oxygen fluence (AO), VUV radiation dose and number of impacts by micrometeoroids/debris vary with θ. Thus it should be possible to assess material degradation and property changes with θ for those materials that are common to three or more locations. Once the θ-dependence functions have been defined, other material sample data from any location can then be used to predict damage and property changes as a function of θ as well.

Table 1 summarizes the polymer matrix composite samples analysed at UTIAS. It can be seen that they were distributed over seven circumferential locations around LDEF. Also shown is the variation in atomic oxygen fluence (atoms/cm^2) and the total VUV radiation exposure at each location, measured in *equivalent sun hours* (ESH). It should be noted that one material (934/T300) was present at seven of the locations.

The properties that were measured include the solar absorptance (α_s), the infrared emittance (ε) and the erosion depth. Tables 2a, 2b and 2c summarize all the data obtained from these samples.

SOLAR ABSORPTANCE (α_s) AND INFRARED EMITTANCE (ε)

Measurement Procedures

Absorptance and emittance measurements were carried out on all samples received. Absorptance measurements were performed using a Beckman DK-2A integrating sphere ratio recording spectrophotometer with a magnesium oxide reference. Solar absorptance is calculated from the relative absorptance spectrum, according to ASTM E 424 and ASTM E 903, across the range of 250 to 2400 nm. IR emittance was measured using a Gier-Dunkle DB100 infrared reflectometer with appropriate calibrating standards and in accordance with ASTM E 408.

Experimental Results

Tables 3 and 4 present the solar absorptance (α_s) and emittance data (ε) for the materials investigated, including the differences found between the exposed and unexposed faces. A plot of the solar absorptance change (%) in Fig. 2 shows a maximum increase at or near the ram direction on all samples, coincident with maximum AO and UV degradation on the ram side. As θ increases, the absorptance quickly drops to values which are less than the back face reference values, well before θ = 90°. It was expected that α would only decrease to some value slightly higher than the "control" at or near 90°, since thermal AO and UV radiation degrades surfaces, to some extent, at all locations around the satellite. This unexpected result indicates that some other mechanism must be altering the surface characteristics, one that is not related to AO or UV surface degradation.

Contamination of the surface by vacuum-condensable silicone-based molecular compounds has been measured all over LDEF (ref. 1). The presence of this material on the surface would be consistent with a reduction in α for a high α material such as a graphite fibre composite. The contaminant tends to be light brown or tan in colour.

It is likely that, for these black graphite-based PMC's, the AO flux dropped low enough for contamination to build up between 60° and 80°. At angles less than 60°, the AO flux was high enough to remove the molecular contamination as it formed. At angles greater than approximately 80°, the flux was too low to remove all of the contaminant as it formed on the surface. Visual examination, IR and EDX spectra are inconclusive as to the presence of any uniform contamination on these rough sample surfaces. The contamination is clearly visible on aluminum portions of the trays and end fittings near the samples. Other work, specifically on contamination, has shown the brownish contamination at these higher θ angles (ref. 2).

A related effect can be seen in the emittance vs θ plot of Fig. 3. As expected, there is an increase in emittance of the samples subjected to ram AO and UV radiation. At higher θ's, emittance decreases to values below the control (i.e., back face value). At the highest θ angles, however, emittance returns to the control value. The initial decrease in emittance appears to occur in the same range as the absorptance decrease, which means that the same AO erosion/contamination mechanism should apply. The return to control values at the highest θ angles indicates that the increase in UV irradiation on the trailing edge may be increasing the emittance of the samples. These results can be compared to α measurements for Al clamps and FEP/Ag from other experiments. Emittance effects are not as clear since the changes were quite small (refs. 3, 4).

Measurements made on FEP/Ag samples from the UHCRE (Ultra-Heavy Cosmic Ray Nuclei Experiment) show the same pattern of increase in absorptance at the leading edge, a decrease below the control value, but with a rapid increase on the trailing sides [3]. Here UV degradation dominates, increasing α at the leading and trailing edges while contamination probably lowers the absorptance below the control, around 90°.

Boeing's chromic acid anodized aluminum clamp measurements show the same basic effect [4]. In this case, absorptance decreases at high AO/UV flux levels, while the brown contamination increases absorptance. Again, contamination forces the α change beyond the control value. The transition from AO/UV effect to contamination effect occurs at 90° this time.

ATOMIC OXYGEN EROSION

The atomic oxygen fluence as a function of angular location around LDEF is summarized in Table 1. Although most of the angular variation can be described by a simple 'cosine' function, it is known that because of the random thermal motion associated with the AO, some exposure occurs well beyond the 90° position (ref. 5).

Summaries of the erosion depth measurements for the materials investigated at UTIAS, together with published data, are presented in Tables 5a and 5b, respectively. Cross-sectional SEM measurements were made at UTIAS to obtain the erosion loss. A plot of this data as a function of θ is given in Fig. 4. SEM micrographs illustrating the differences in erosion morphologies are given in Figs. 5 and 6 for 934/T300 graphite/epoxy samples located at 8° and 82°, respectively.

Cross-sectional SEM micrographs are shown in Figs. 7 and 8. Of special interest are the erosion depth profiles (when compared to the unexposed regions shown) and the relatively large surface 'pits,' probably caused by microparticle impacts.

In Fig. 9, it can be seen that a $\cos^{1.5}\theta$ function fits the 934/T300 erosion data rather well, except in the range of $\theta = 82°$. Erosion is much larger than expected at this angle location. It has been previously noted that "significant differences" at high angles on FEP/Ag have also been measured (ref. 6). It is likely that surface morphology has an important effect by trapping incoming AO and increasing the probability of surface interaction. Large increases in interaction probability have been demonstrated as undercutting effects by Banks et al (ref. 7).

One can calculate the erosion yield as a function of angular location, $Y(\theta)$, from the relation $Y(\theta) = \frac{\text{erosion depth}}{\text{AO fluence}}$ (cm^3/atom). A summary of these values is given in Tables 5a and 5b. For design purposes, it is more convenient to work with the "normal" erosion yield parameter (Y_n), i.e., the value of Y that one would measure for a material whose plane was normal to the incident AO flux, $Y_n = Y(\theta)/\cos^m\theta$.

Tables 5a and 5b present the values of Y_n for m = 0.5. It is clear from Table 5a for the $\theta = 82°$ data, that Y_n is far too high for epoxy-based composites. Since half of the erosion depth recorded at $\theta = 82°$ was accounted for by an outer epoxy layer, one would indeed expect an erosion yield to be higher than that for the bulk graphite/epoxy material, but not as high as the values shown. Using a value of m = 0.2 gave Y_n results much lower at $\theta = 82°$, although not significantly lower for the smaller values of θ

(see Table 5a and Fig. 9). Included in Fig. 10 is a correction factor for the effect of a 10μ epoxy layer (as measured from the UTIAS samples located at $\theta = 82°$).

A plot of the normal erosion yield values (Y_n) based on m = 0.2 is presented in Fig. 10. It is clear that for $0 < \theta \leq 70°$ essentially constant yield values are obtained, independent of angular location θ because of the larger erosion losses that occurred. For these samples, one is essentially measuring a bulk property not significantly affected by the outer epoxy layer. However, for smaller erosion depths, a larger value for Y_n is obtained, consistent with the effect of the epoxy layer.

An estimate of the total erosion loss (h) for a polymer matrix composite laminate oriented at an angle θ to an incident normal AO flux (ϕ_n) for a given time 't' is given by $h(\theta,t) = Y_{nc}\phi_n t(\cos\theta)^{1+m} + h_r\left(1 - \frac{Y_{nc}}{Y_{nr}}\right)$, where Y_{nc}, Y_{nr} are the normal erosion yields for the bulk composite and outer resin layer (of thickness h_r), respectively.

THE ROLE OF CHEMICAL CONTENT ON THE EROSION OF HYDROCARBON POLYMERS

A study was conducted to establish a relationship between the atomic oxygen erosion rate of hydrocarbon-based polymers and their chemical content and structure. Based on a comprehensive analysis of erosion data for a large number of samples exposed to the low Earth orbit (LEO) space environment and to simulated LEO environment conditions in ground-based hyperthermal facilities, an excellent linear correlation exists between the AO erosion rate and a structural parameter γ defined as the ratio of total number of atoms in a repeat monomer unit to the difference between the total carbon content and the total number of intermolecular oxygen in the same repeat unit, i.e., the relative content of effective carbon atoms in it (Fig. 11). The structural parameter γ actually represents the chemical content of the material, or the relative content of "effective carbon atoms." It would appear that the removal of these "effective carbon atoms" by oxidation is the limiting step for erosion by fast atomic oxygen. Figure 12 provides examples of three polymer materials and the calculation of γ.

CONCLUSIONS

1. Increases in solar absorptance and infrared emittance relative to control values have been measured as high as +12% and +18%, respectively in the ram direction. Absorptance decreased to slightly below the "control" value around $\theta \approx 60°$, whereas the emittance decrease was as great as -12% in the range of $60 < \theta < 120°$, rising again to the nominal "control" value for $160 \leq \theta \leq 180°$.

2. The erosion loss has been found to vary around the circumference as $\cos^{0.5}\theta$ over much of the range of θ. However, at large θ values (i.e., $\theta > 70°$), a better approximation is given by $\cos^{0.2}\theta$. Incorporating the effect of the outer epoxy layer yields a better estimate of erosion. Enhanced erosion at large θ angles is postulated to occur because of AO trapping resulting from the surface morphology and the increased reaction probability.

3. The average bulk normal erosion yield (Y_{nc}) for the fourteen different composite materials is $\sim 1 \times 10^{-24}$ cm3/atom based on a $\cos^{0.2}\theta$ relation (neglecting the 82° epoxy-dominated data and the

three questionable values in Tables 5a and 5b). The range of values measured for these various materials is given by $0.76 \leq Y_{nc} \leq 1.2 \times 10^{-24}$ cm^3/atom.

4. The erosion yield for hydrocarbon-based polymers exposed to hyperthermal atomic oxygen has been found to vary linearly with a chemical structure/content parameter γ. This functional relationship is useful for designing new materials in terms of their resistance to AO.

ACKNOWLEDGEMENT

The analysis of LDEF data and research results presented in this report were financed by the Space Mechanics Directorate of the Canadian Space Agency, under Contract No. 025SR.9 F009-1-1435, FC 5305-001-65 301-201-1400. Special thanks are given to Dr. D. G. Zimcik, Space Mechanics Directorate, Canadian Space Agency, for his support of this program. The authors also wish to recognize the efforts of Mr. G. Manuelpillai and Dr. W. D. Morison for their contributions to this research project. We all extend our thanks to the many LDEF investigators and their organizations who supplied us with LDEF samples for analysis. They include: Mr. Christopher Blair, Lockheed Missiles and Space Co.; Dr. David K. Felbeck, University of Michigan; Mr. Pete E. George and Mr. Harry Dursch, Boeing Defense and Space Group; Mr. Dick Vyhnal, Rockwell International; Mr. Thomas Cookson, General Dynamics Space Systems; and Mr. Charles A. Smith, McDonnell Douglas.

The study of the erosion of hydrocarbon polymers and the development of the $Y_n(\gamma)$ graph was done in collaboration with Dr. Z. Iskanderova (UTIAS), Dr. Y. I. Gudimenko (Academy of Sciences, Institute of Physical Organic Chemistry, Minsk, Belarus), and Dr. J. Kleiman (UTIAS).

REFERENCES

1. G. A. Harvey, "Organic Contamination of LDEF," LDEF-69 Months in Space, Part 1, NASA Conference Publication 3134, June 1991, 179.

2. E. R. Crucher and K. J. Warner, "Molecular Films Associated with LDEF," LDEF — 69 Months in Space, Part 1, NASA Conference Publication 3134, June 1991, 155.

3. F. Levadou et al, "Preliminary Investigations into UHCRE Thermal Control Materials," LDEF — 69 Months in Space, Part 2, NASA Conference Publication 3134, June 1991, 875.

4. W. L. Plagemann, "Space Environmental Effects on the Integrity of Chromic Acid Anodized Coatings," LDEF — 69 Months in Space, Part 2, NASA Conference Publication 3134, June 1991, 1023.

5. R. J. Bourassa, J. R. Gillis, "LDEF Atomic Oxygen Flux and Fluence Calculations," NASA LDEF MSIG Report NAS1-18224, Task 12, January 1991.

6. B. A. Banks et al, "Atomic Oxygen Interactions with FEP Teflon and Silicones on LDEF," LDEF — 69 Months in Space, Part 2, NASA Conference Publication 3134, June 1991, 801.

7. B. A. Banks, S. K. Rutledge, B. M. Auer and F. Di Filippo, "Atomic Oxygen Undercutting of Defects on SiO_2 Protected Polyimide Solar Array Blankets," Proc. Materials Degradation in Low Earth Orbit, The Minerals, Metals and Materials Society, 1990, 15.

8. P. E. George and S. G. Hill, "Results from Analysis of Boeing Composite Specimens Flown on LDEF Experiment M0003," LDEF-69 Months in Space, First Post-Retrieval Symposium, June 2-8, 1991, NASA CP-3134, Part 2, p. 1115.

9. G. L. Steckel and T. D. Le, "M0003-10: LDEF Advanced Composites Experiment," LDEF — 69 Months in Space, First Post-Retrieval Symposium, June 2-8, 1991, NASA CP-3134, Part 2, p. 1041.

10. W. S. Slemp, P. R. Young, G. W. Witte Jr., and J. Y. Shen, "Effects of LDEF Flight Exposure on Selected Polymer Matrix Resin Composite Materials," LDEF — 69 Months in Space, First Post-Retrieval Symposium, June 2-8, 1991, NASA CP-3134, Part 2, p. 1149.

11. A. F. Whitaker and L. E. Young, "An Overview of the First Results on the Solar Array Materials Passive LDEF Experiment (SAMPLE), AO171," LDEF — 69 Months in Space, First Post-Retrieval Symposium, June 2-8, 1991, NASA CP-3134, Part 3, p. 1241.

Table 1

Samples Collected - θ Project

Material	Row	Angle	AO Fluence (atom/cm^3)	UV Dose (ESH)	Laminate	#	
P1700/T300	3	172	1.32×10^{17}	11100	$(0°,90°)_4$	1	Boeing
CE339/GY70					$(0°)_2,(90°)_2$	1	Lockheed
934/T300					0°	1	Boeing
PES-C/T300						1	M. Doug.
P1700/T300	4	158	2.31×10^{5}	10400	$(0°,90°)_4$	1	Boeing
F593/P75					$(0°)_{16}$	1	Lockheed
934/T300					0°	1	Boeing
934/T300	1	112	2.92×10^{17}	7500	Honeycomb	1	Rockwell
934/T300					$(45°,(0°)_8)_2,45°$	1	Rockwell
934/T300	12	82	1.33×10^{21}	6900	$(0°)_4$	1	UTIAS
5208/T300					$(\pm 45°)_s$	1	UTIAS
5208/T300					$(\pm 20°)_4$	1	U of Mich
PMR15/C6000	7	68	3.28×10^{21}	7200	$(0°,\pm 45°,90°)_{s2}$	1	Rockwell
F593/P75	8	38	6.93×10^{21}	9400	$(0°)_{16}$	4	Lockheed
PS-C/T300						1	M. Doug.
PES-C/T300						1	M. Doug.
CE339/GY70						2	Gen. Dyn.
934/T300						2	Gen. Dyn
934/T300					0°	1	Boeing
P1700/T300	9	8	8.99×10^{21}	11100	$(0°,90°)_4$	1	Boeing
CE339/GY70					$(0°)_2,(90°)_2$	1	Lockheed
934/T300					0°	1	Boeing

Table 2a

UTIAS Samples

Measured Values

Material	Row	Angle	AO Fluence (atoms/cm^2)	UV Dose (ESH)	#	Solar Absorpt. - Front -	- Back -	IR Emit. - Front -	- Back -	AO Erosion Depth (microns)	Matrix * Microcracking
934/T300	12	82	1.33E+21	6900	1	0.814	0.830	0.703	0.796	21.5	None Observed
5208/T300	12	82	1.33E+21	6900	1	0.872	0.883	0.706	0.804	17.7	None Observed

* Does not include manufacturing process induced cracking

Lockheed Samples

Measured Values

Material	Row	Angle	AO Fluence (atoms/cm^2)	UV Dose (ESH)	#	Solar Absorpt. - Front -	- Back -	IR Emit. - Front -	- Back -	AO Erosion Depth (microns)	Matrix * Microcracking
CE339/GY70	9	8	8.99E+21	11100	1	0.985	0.881	0.918	0.805	65.4	None Observed
CE339/GY70	3	172	1.32E+17	11100	1	0.857	0.884	0.800	0.787	None	None Observed
F593/P75	8	38	6.93E+21	9400	4	Not Used Yet - Preserved for CTE/Outgas Testing					
F593/P75	4	158	2.31E+05	10400	1						

Rockwell Samples

Measured Values

Material	Row	Angle	AO Fluence (atoms/cm^2)	UV Dose (ESH)	#	Solar Absorpt. - Front -	- Back -	IR Emit. - Front -	- Back -	AO Erosion Depth (microns)	Matrix * Microcracking
934/T300	1	112	2.92E+17	7500	1	0.886	0.896	0.790	0.870	None	None Observed
934/T300	1	112	2.92E+17	7500	1	Composite in honeycomb, not used for these properties					
PMR15/C6000	7	68	3.28E+21	7200	1	0.876	0.899	0.750	0.840	30.1	None Observed

Table 2b

Boeing Samples

Measured Values

Material	Row	Angle	AO Fluence (atoms/cm^2)	UV Dose (ESH)	#	Solar Absorpt. - Front -	- Back -	IR Emit. - Front -	- Back -	AO Erosion Depth (microns)	Matrix * Microcracking
934/T300	9	8	8.99E+21	11200	1	0.943	0.835	0.943	0.835	NA	N/A **
934/T300	8	38	6.93E+21	9400	1	0.886	0.832	0.886	0.832	NA	N/A
934/T300	3	172	1.32E+17	11100	1	0.769	0.804	0.769	0.804	None	N/A
934/T300	4	158	2.31E+05	10500	1	0.832	0.819	0.832	0.819	None	N/A
P1700/T300	9	8	8.99E+21	11200	1	0.983	0.895	0.983	0.895	NA	N/A
P1700/T300	3	172	1.32E+17	11100	1	0.871	0.889	0.871	0.889	None	N/A
P1700/T300	4	158	2.31E+05	10500	1	0.873	0.881	0.873	0.881	None	N/A

** samples mechanically tested previous to cross-sectioning

U of Mich. Sample

Measured Values

Material	Row	Angle	AO Fluence (atoms/cm^2)	UV Dose (ESH)	#	Solar Absorpt. - Front -	- Back -	IR Emit. - Front -	- Back -	AO Erosion Depth (microns)	Matrix * Microcracking
5208/T300	12	82	1.33E+21	6800	1	0.857	0.859	0.665	0.627	NA	None Observed

Table 2c

General Dynamics Samples

Measured Values

Material	Row	Angle	AO Fluence (atoms/cm^2)	UV Dose (ESH)	#	Solar Absorpt. - Front -	- Back -	IR Emit. - Front -	- Back -	AO Erosion Depth (microns)	Matrix * Microcracking
CE339/GY70	8	38	6.93E+21	9400	1					56.3	None Observed
CE339/GY70	8	38	6.93E+21	9400	1					50.0	None Observed
934/T300	8	38	6.93E+21	9400	1					61.3	None Observed
934/T300	8	38	6.93E+21	9400	1					60.0	None Observed

Absorptance and emittance measurements not performed due to small size

McDonnell Douglas Samples

Measured Values

Material	Row	Angle	AO Fluence (atoms/cm^2)	UV Dose (ESH)	#	Solar Absorpt. - Front -	- Back -	IR Emit. - Front -	- Back -	AO Erosion Depth (microns)	Matrix * Microcracking
PS-C/T300	8	38	6.93E+21	9400	1					65.0	Extensive
PS-C/T300	3	172	1.32E+17	11100	1					none	None Observed
PES-C/T300	8	38	6.93E+21	9400	1					55.0	None Observed

Absorptance and emittance measurements not performed due to small size

Table 3

Solar Absorptance Comparison

	Material	Front	Back	Difference	% difference	Angle
UTIAS	934/T300	0.814	0.830	-0.016	-1.9%	82
	5208/T300	0.872	0.883	-0.011	-1.2%	82
Lockheed	CE339/GY70	0.985	0.881	0.104	11.8%	8
	CE339/GY70	0.857	0.884	-0.027	-3.1%	172
Rockwell	934/T300	0.886	0.896	-0.010	-1.1%	112
	PMR15/C6000	0.876	0.899	-0.023	-2.6%	68
Boeing	934/T300	0.955	0.863	0.092	10.7%	8
		0.918	0.865	0.053	6.1%	38
		0.861	0.877	-0.016	-1.8%	172
		0.867	0.875	-0.008	-0.9%	158
	PMR15/C6000	0.980	0.910	0.070	7.7%	8
	PMR15/C6000	0.900	0.910	-0.010	-1.1%	172
	P1700/T300	0.983	0.895	0.088	9.8%	8
		0.871	0.889	-0.018	-2.0%	172
		0.873	0.881	-0.008	-0.9%	158
U of Mich.	5208/T300	0.857	0.859	-0.002	-0.2%	82

Table 4

Emittance Comparison

	Material	Front	Back	Difference	% Difference	Angle
UTIAS	934/T300	0.703	0.796	-0.093	-11.7%	82
	5208/T300	0.706	0.804	-0.098	-12.2%	82
Lockheed	CE339/GY70	0.918	0.805	0.113	14.0%	8
	CE339/GY70	0.800	0.787	0.013	1.7%	172
Rockwell	934/T300	0.790	0.870	-0.080	-9.2%	112
	PMR15/C6000	0.750	0.840	-0.090	-10.7%	68
Boeing	934/T300	0.943	0.835	0.108	12.9%	8
		0.886	0.832	0.054	6.5%	38
	934/T300	0.769	0.804	-0.035	-4.4%	172
		0.832	0.819	0.013	1.6%	158
	PMR15/C6000	0.930	0.790	0.140	17.7%	8
	PMR15/C6000	0.790	0.830	-0.040	-4.8%	172
	P1700/T300	0.922	0.822	0.100	12.2%	8
		0.817	0.825	-0.008	-1.0%	172
		0.806	0.803	0.003	0.4%	158
U of Mich.	5208/T300	0.665	0.627	0.038	6.1%	82

Table 5a

Erosion Yields - Various angles - As measured

Material	Row	Angle (deg)	Fluence (atom/cm ^ 2)	Depth (micron)	Y(θ) (cm ^ 3/atom)	Yn cos ^ 0.5 (cm ^ 3/atom)	Yn cos ^ 0.2 (cm ^ 3/atom)	Type	Source
934/T300	12	82	1.33E+21	21.5	1.6E-24	4.3E-24	2.4E-24	Ep/Gr	UTIAS
5208/T300	12	82	1.33E+21	17.7	1.3E-24	3.6E-24	2.0E-24	Ep/Gr	UTIAS
5208/T300	12	82	1.33E+21	20.1	1.5E-24	4.1E-24	2.2E-24	Ep/Gr	U. of Mich
CE339/GY70	9	8	8.99E+21	65.4*	7.3E-25	7.3E-25	7.3E-25	Ep/Gr	Lockheed
934/T300	9	8	8.99E+21	90.7	1.0E-24	1.0E-24	1.0E-24	Ep/Gr	Boeing
P1700/T300	9	8	8.99E+21	94.0	1.0E-24	1.1E-24	1.0E-24	Polysulfone/Gr	Boeing
934/T300	8	38	6.93E+21	82.2	1.2E-24	1.3E-24	1.0E-24	Ep/Gr	Boeing
PS-C/T300	8	38	6.93E+21	65.0	9.4E-25	1.1E-24	9.8E-25	Polysulfone/Gr	McDonnell Douglas
PES-C/T300	8	38	6.93E+21	55.0	7.9E-25	8.9E-25	8.3E-25	P-ethersulfone/Gr	McDonnell Douglas
CE339/GY70	8	38	6.93E+21	56.3	8.1E-25	9.2E-25	8.5E-25	Ep/Gr	General Dynamics
CE339/GY70	8	38	6.93E+21	50.1	7.2E-25	8.1E-25	7.6E-25	Ep/Gr	General Dynamics
934/T300	8	38	6.93E+21	61.3	8.8E-25	1.0E-24	9.3E-25	Ep/Gr	General Dynamics
934/T300	8	38	6.93E+21	60.0	8.7E-25	9.8E-25	9.1E-25	Ep/Gr	General Dynamics
PMR15/C6000	7	68	3.39E+21	30.1	8.9E-25	1.5E-24	1.1E-24	Polyimide/Gr	Rockwell

* Large surface erosion grooves

Table 5b

Erosion Yields — Various Angles — From Literature

Material	Row	Angle (deg)	Fluence (atom/cm ^ 2)	Depth (micron)	Y (θ) (cm ^ 3/atom)	Y_n cos ^ 0.5 (cm ^ 3/atom)	Y_n cos ^ 0.2 (cm ^ 3/atom)	Type	Source†
PMR15/C6000	9	8	8.99E+21	112.0	1.2E-24	1.3E-24	1.2E-24	Polyimide/Gr	Boeing
5208/T300	9	8	8.99E+21	114.3**	1.3E-24	1.3E-24	1.3E-24	Ep/Gr	NASA LaRC AO134
P1700/C6000	9	8	8.99E+21	76.2	8.5E-25	8.5E-25	8.5E-25	Polysulfone/Gr	NASA LaRC AO134
CE339/P75S	8	38	6.93E+21	78.0	1.1E-24	1.3E-24	1.2E-24	Ep/Gr	Aerospace Corp.
CE339/GY70	8	38	6.93E+21	75.0	1.1E-24	1.2E-24	1.1E-24	Ep/Gr	Aerospace Corp.
934/P75S	8	38	6.93E+21	55.0	7.9E-25	8.9E-25	8.3E-25	Ep/Gr	Aerospace Corp.
934/GY70	8	38	6.93E+21	60.5	8.7E-25	9.8E-25	9.2E-25	Ep/Gr	Aerospace Corp.
P1700/HMF322	8	38	6.93E+21	110.0*	1.6E-24	1.8E-24	1.7E-24	Polysulfone/Gr	MSFC AO171
934/P75S	8	38	6.93E+21	71.1	1.0E-24	1.2E-24	1.1E-24	Ep/Gr	MSFC AO171
934/HMS	8	38	6.93E+21	68.6	9.9E-25	1.1E-24	1.0E-24	Ep/Gr	MSFC AO171

*Possible contamination

**Measurement technique unknown

†See References 8 to 11

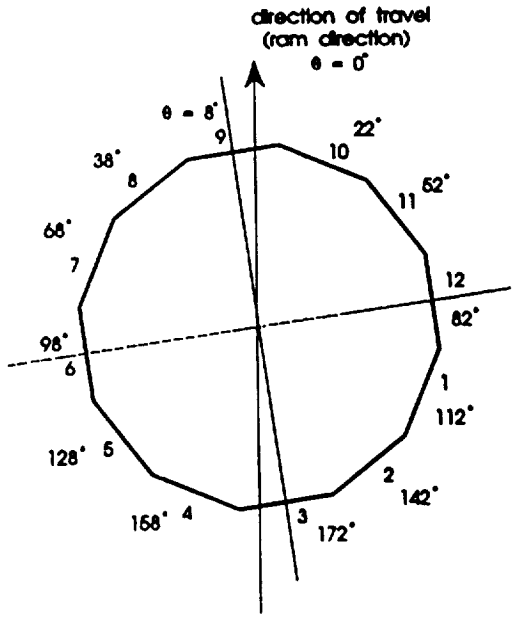

Figure 1. Circumferential Location

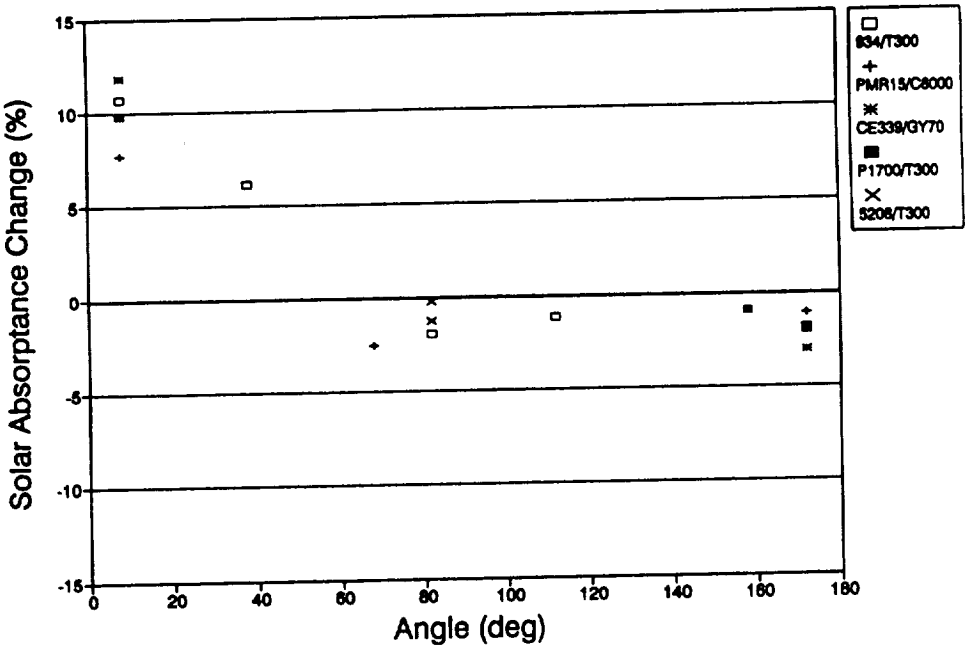

Figure 2. Percent Change in Solar Absorptance

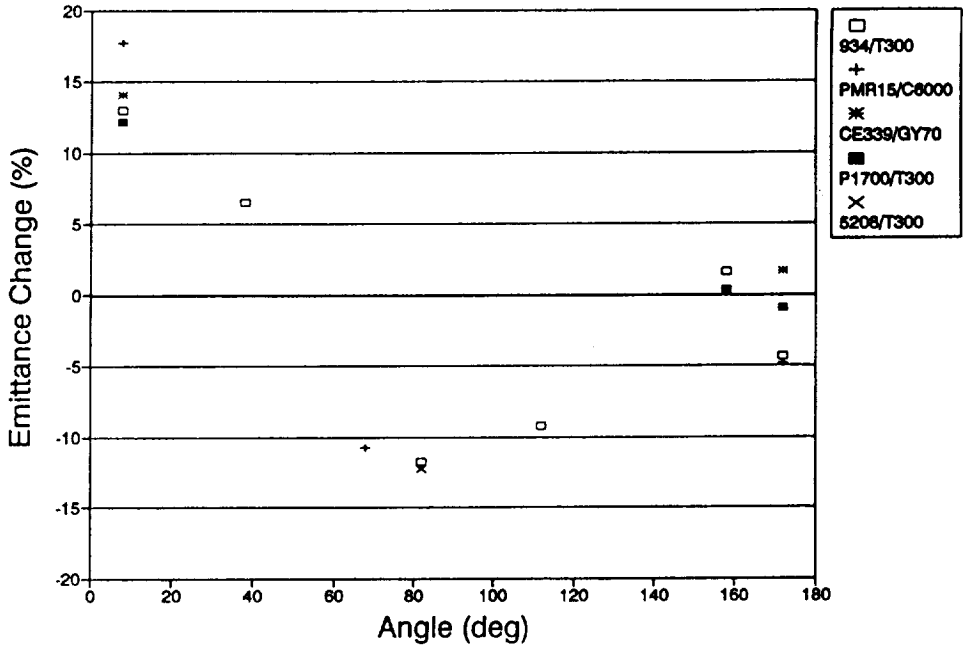

Figure 3. Percent Change in Emittance

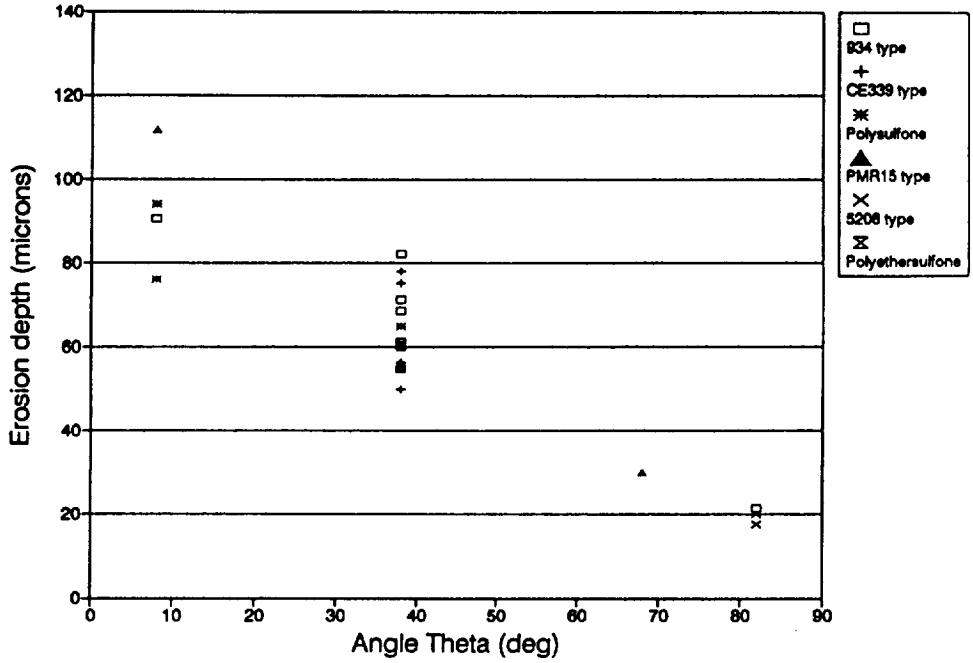

Figure 4. Erosion Depth of PMC Materials

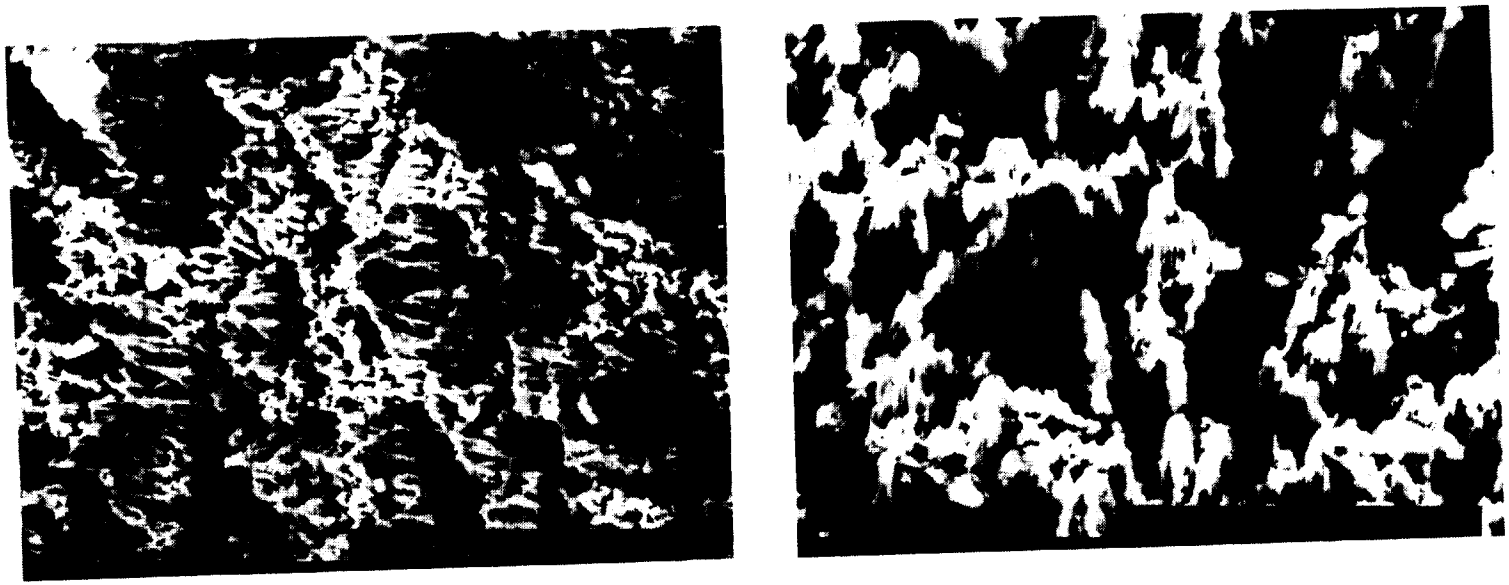

Fig. 5 Erosion of Graphite/Epoxy (T300/934) Material at 8°
(Ref: Boeing...) x750

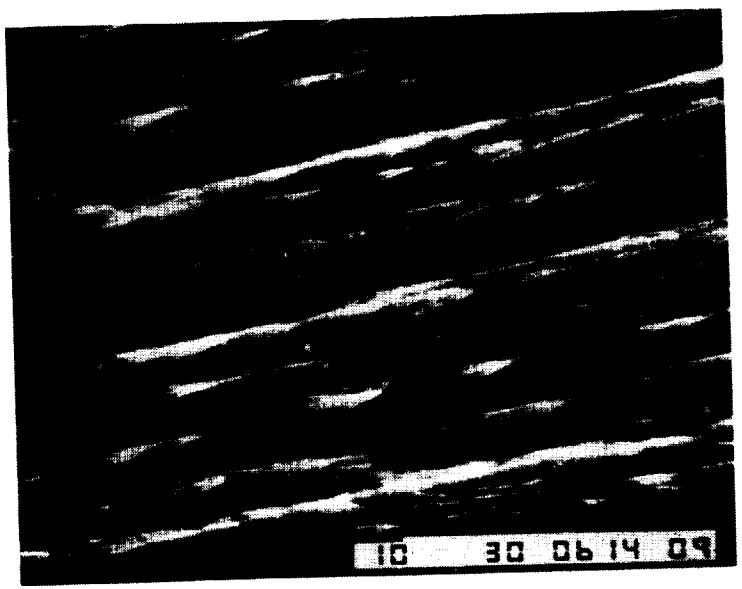

Fig. 6 SEM Photograph of Exposed Area of Graphite/Epoxy Laminate
(934/T300: $(\pm 45°)_s$ at 82° (UTIAS) x750

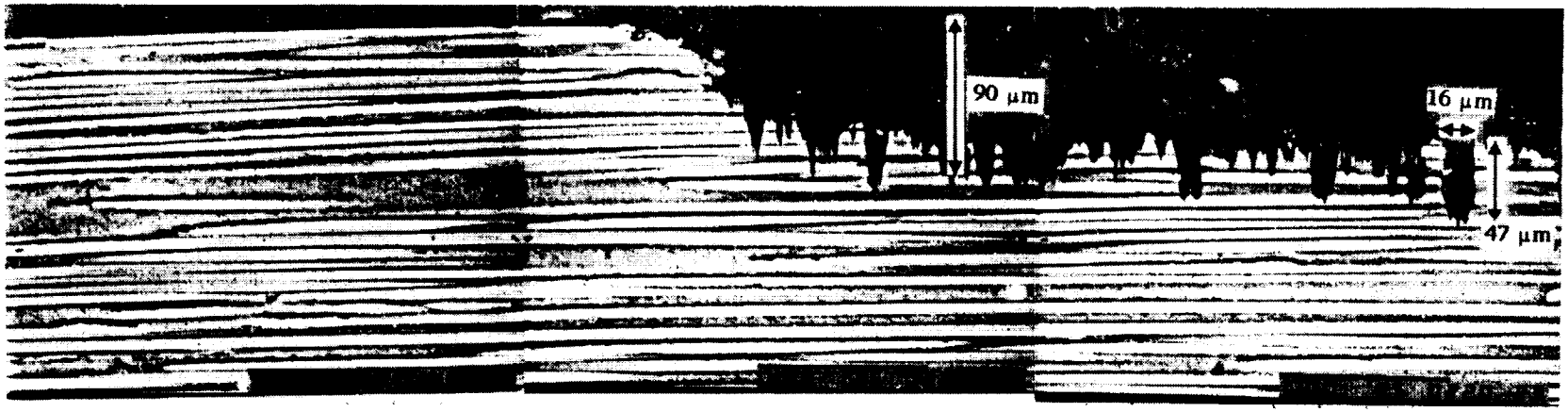

Fig. 7 SEM Micrograph Cross-Section of 934/T300 (0°) from RAM side showing
Shielded Edge and the Effect of AO Erosion at 8° (Ref. Boeing...)

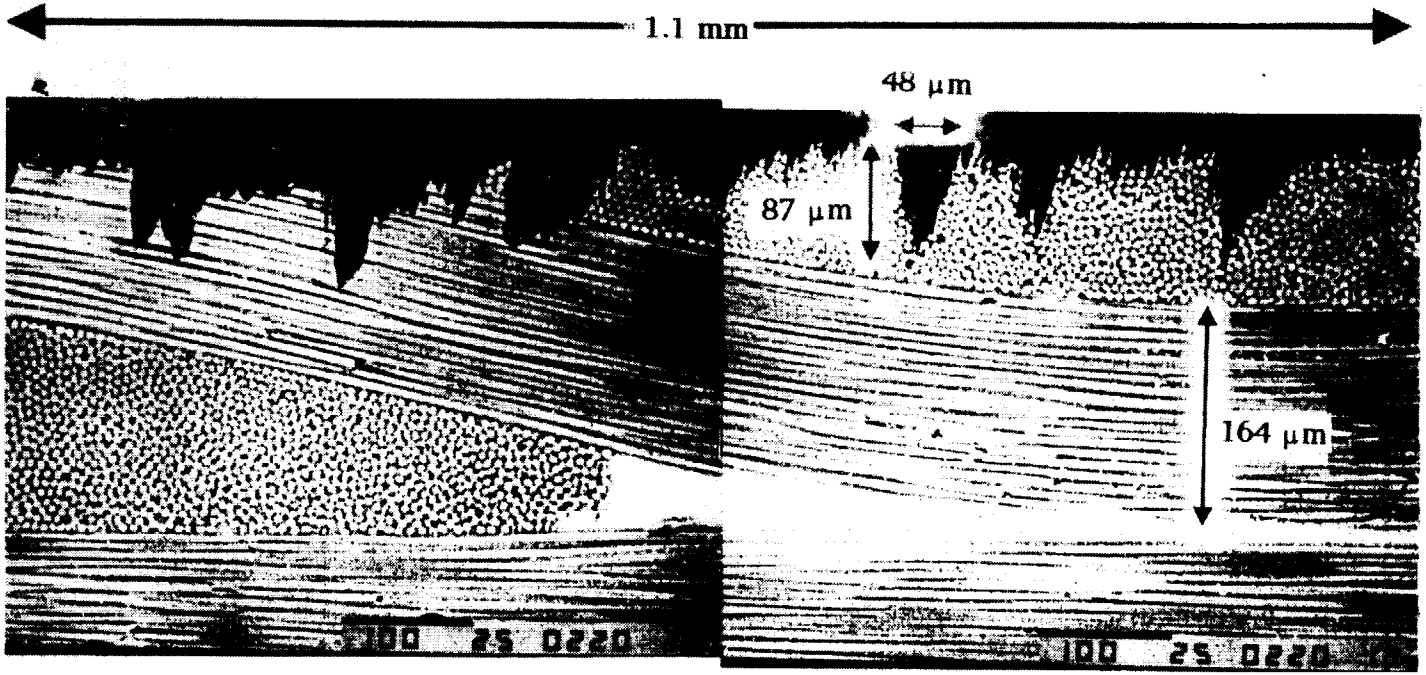

Fig. 8 SEM Micrograph of P1700/T300 Polysulfone/Graphite Cross-Section showing
Eroded Section and Micro-particle Impact Sites
Location: Row 9 (8° off Ram) Layup: $(0, 90)_4$ Fabric (Ref: Boeing...)

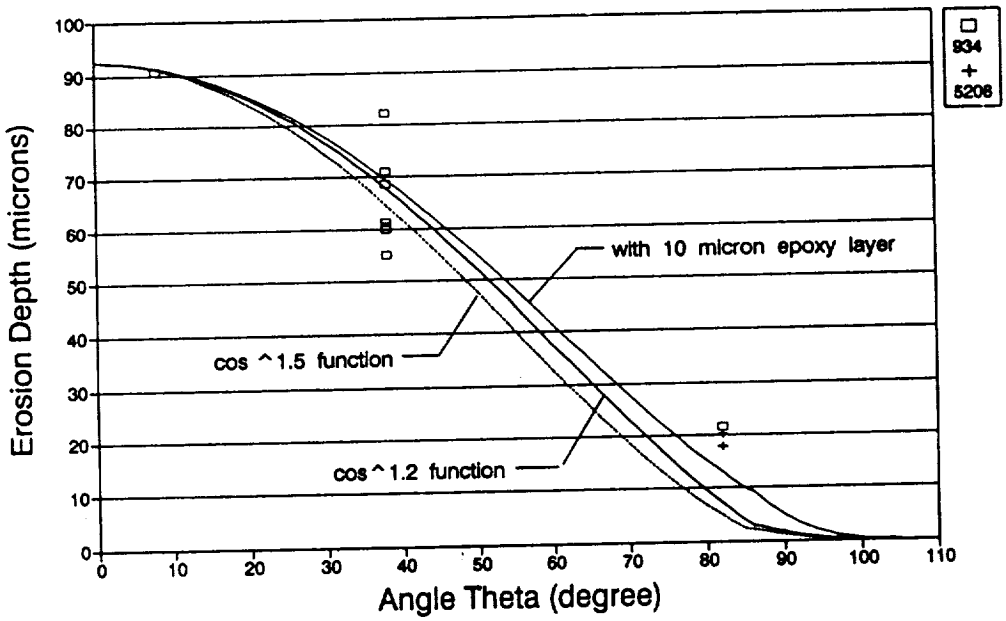

Figure 9. Erosion Depth of Epoxy Type Composite Samples - Epoxy Layer Effect

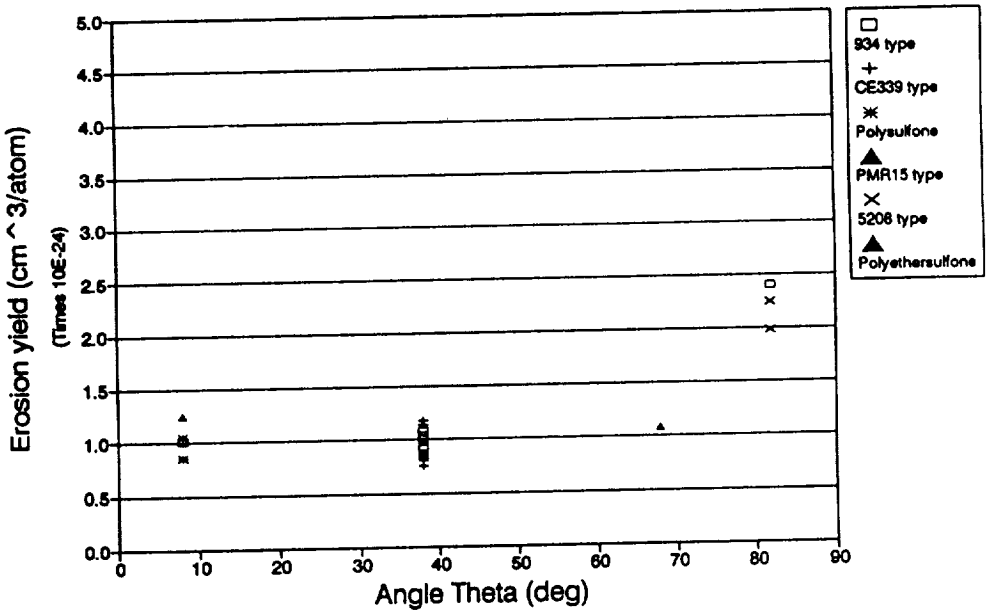

Figure 10. Normal Erosion Yield (Y_n) cos ^ 0.2

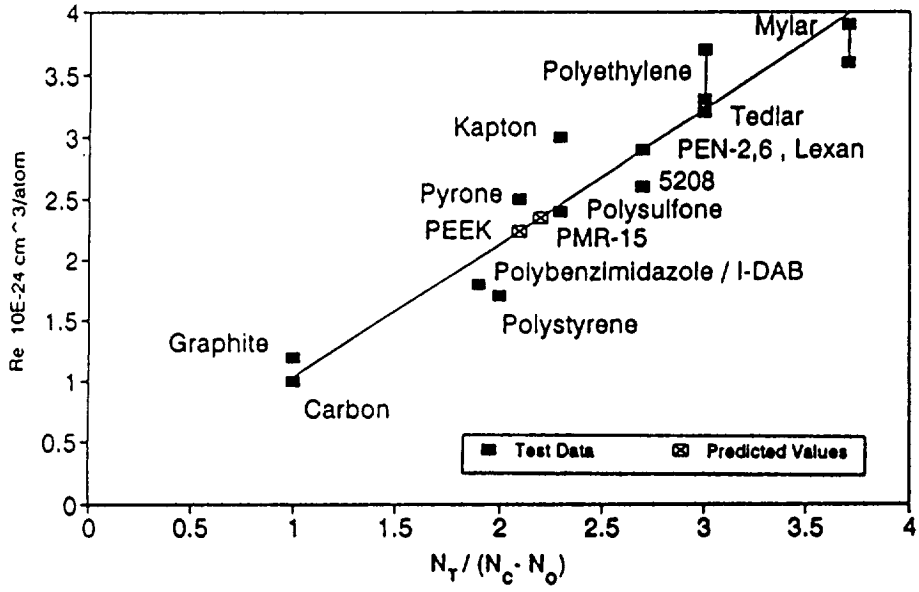

Figure 11. Effect of Polymer Structure on Erosion Yield in Presence of Hyperthermal Atomic Oxygen (2~5 eV).
Z. A. Iskanderova, Yu. I. Gudimenko, J. I. Kleiman, and R. C. Tennyson

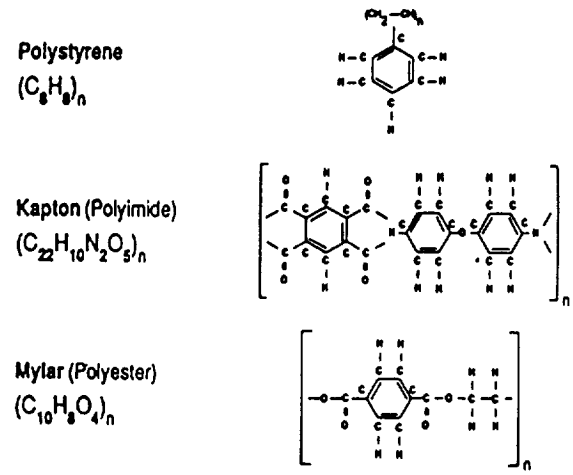

POLYMERS	N_T	N_C	N_O	$\gamma = N_T / (N_C - N_O)$
Polystyrene	16	8	0	16/8 = 2
Kapton (Polyimide)	39	22	5	39/17 = 2.3
Mylar (Polyester)	22	10	4	22/6 = 3.7

N_T = Total number of atoms N_C = number of C atoms N_O = number of O atoms

Figure 12. Examples of Polymer Structures and Calculations of $N_T/(N_C-N_O)$.